



Laser Printing-Enabled Direct Creation of Cellular Heterogeneity in Lab-on-a-Chip Devices

Journal:	<i>Lab on a Chip</i>
Manuscript ID	LC-ART-02-2019-000117.R1
Article Type:	Paper
Date Submitted by the Author:	05-Mar-2019
Complete List of Authors:	Xiong, Ruitong; University of Florida, Department of Mechanical and Aerospace Engineering Chai, Wenxuan; University of Florida, Department of Mechanical and Aerospace Engineering Huang, Yong; University of Florida, Department of Mechanical and Aerospace Engineering

Laser Printing-Enabled Direct Creation of Cellular Heterogeneity in Lab-on-a-Chip Devices

Ruitong Xiong¹, Wenxuan Chai¹, Yong Huang^{1,2,3, *}

¹Department of Mechanical and Aerospace Engineering, University of Florida, Gainesville, FL 32611, USA.

²Department of Materials Science and Engineering, University of Florida, Gainesville, FL 32611, USA.

³Department of Biomedical Engineering, University of Florida, Gainesville, FL 32611, USA.

*Corresponding author, Department of Mechanical and Aerospace Engineering, University of Florida, Gainesville, FL 32611, USA, Phone: 001-352-392-5520, Fax: 001- 352-392-7303,

Email: yongh@ufl.edu

Abstract

Lab-on-a-chip devices, capable of culturing living cells in continuously perfused, micrometer-sized channels, have been intensively investigated to model physiological microenvironments for cell-related testing and evaluation applications. Various chemical, physical, and/or biological culture cues are usually expected in a designed chip to mimic the *in vivo* environment with defined spatial heterogeneity of cells and biomaterials. To create such heterogeneity within a given chip, typical methods rely heavily on sophisticated fabrication and cell seeding processes, and chips fabricated with these methods are difficult to readily adapt for other applications. In this study, laser-induced forward transfer (LIFT)-based printing has been implemented to create heterogeneous cellular patterns in a lab-on-a-chip device to achieve the efficiency in creating heterogeneous cellular patterns as well as the flexibility in adapting different evaluation configurations in lab-on-a-chip devices. Two applications, parallel evaluation of cellular

behavior and targeted drug delivery to cancer cells, have been implemented as proof-of-concept demonstrations of the proposed fabrication method. For the first application, the morphology of cells in different extracellular matrix (ECM) materials cultured under varying conditions has been investigated. It is found that less stiff ECM and dynamic culturing are preferred for spreading of fibroblasts. For the second application, different drug carriers have been utilized for targeted delivery of anticancer drugs to breast cancer cells. It is found that targeted drug delivery is important to realize effective chemotherapy and drug release rate from drug carriers affects the chemotherapy effect. Consequently, the proposed laser printing-based method enables direct creation of heterogeneous cellular patterns within lab-on-a-chip devices which improves the efficiency and versatility of cell-related sensing and evaluation using lab-on-a-chip devices.

1. Introduction

Conventional static cell cultures have been widely adopted to develop *in vitro* biological models as an alternative to directly examining the human body and underlying cell and tissue structures *in vivo*.¹ However, most static cell culture models have limited capacities to fully mimic the complex structures and functions of living organs and may not be able to recapitulate some crucial organ-specific variations for cells such as spatiotemporal chemical gradients and mechanical forces in their local tissue microenvironment.² Accordingly, cell-based lab-on-a-chip devices, which are developed based on microfluidic platforms and capable of culturing living cells in continuously perfused, micrometer-sized channels in order to model the physiological microenvironments and functions of tissues and organs³, have been intensively studied in recent years. Such microfluidic-based lab-on-a-chip devices enable precision control of dynamic cellular microenvironments, which are not readily achievable in static cultures or bioreactors,

based on physiological and anatomic requirements of specific organs. In addition, such devices provide necessary functional units to recapitulate tissue- and organ-level functions in cost effective portable format which requires minimal materials and occupies small footprints.^{4,5}

Generally, cells incorporated in lab-on-a-chip devices are either uniformly distributed to form monolayers⁶ and micro-tissues⁷, or heterogeneously deposited in the devices as different cellular patterns⁸. For better understanding of biological events in realistic microenvironments, heterogeneous structures, either in distinct patterns or in direct juxtaposition³, are generally expected. As such, various chemical, physical, and/or biological culture cues have been deposited heterogeneously to mimic the *in vivo* environment by defined spatial heterogeneity of cells and biomaterials. To create such heterogeneity within a given chip, different methods have been utilized such as using the photolithography-based technique to create a self-assembled monolayer (SAM)-modified gold surface to selectively control the adhesion of cells on certain areas¹² and using microfluidic patterning^{9, 10, 13, 14} to seed cells at different compartments on a chip. However, these methods not only rely heavily on delicate surface chemistry treatment or sophisticated photolithography for chip microfabrication¹⁵ but also require an additional cell seeding and material casting step. Moreover, chips fabricated with the above methods are usually uniquely designed to deliver a specific function and are difficult to readily adapt for other applications.

Currently, cell printing technology has been utilized in many biomedical research areas including tissue engineering and regenerative medicine¹⁶⁻¹⁸. For its capability to transfer and pattern cells and biomaterials, it is a promising technique to create spatially heterogeneity of cells and

biomaterials for functional testing and evaluation in lab-on-a-chip devices. Although microfluidic devices¹⁹ and microchannels for perfused cell culture²⁰ have been created by printing-based methods, the printing techniques were mainly used as alternatives to conventional soft lithography or replica molding for the fabrication of channels and devices, and direct printing of cellular patterns for functionality testing and evaluation in lab-on-a-chip devices are to be further explored. Among representative cell printing techniques, laser-assisted printing²¹, developed based on the principle of laser-induced forward transfer (LIFT), is a non-contact droplet-on-demand technique with printing resolution defined by the size of a single droplet (typically on the order of 100 μm). Also, due to its orifice-free nature, laser printing avoids nozzle clogging-related failure while printing with highly-viscous materials or cell-laden bioinks with high cell concentration²². In addition, since it is not necessary to fill the dead zone of cartridges or syringes with printing materials as in orifice-based methods such as inkjetting and extrusion printing, laser printing requires fewer materials and cells when switching between different printing materials. Therefore, laser printing has good potential to print heterogeneous patterns with controllable location, shape and dimension of created patterns from materials with a wide range of viscosity and cell density. In addition, as different patterns can be laser-printed based on testing requirements, it can be applied to create lab-on-a-chip devices with high flexibility to meet with different testing configurations.

The objective of this study is to demonstrate a laser printing-based method to directly create heterogeneous cellular patterns for functional testing in lab-on-a-chip devices. Laser printing improves the efficiency and flexibility of current methods for creating functional heterogeneity on lab-on-a-chip devices for cell-related testing and evaluation applications. A chip has been

developed with the proposed method and two applications, parallel evaluation of cellular behavior and targeted drug delivery to cancer cells, have been implemented as proof-of-concept demonstrations of the proposed method. In particular, the effect of extracellular matrix (ECM) properties and culturing conditions on the fibroblast morphology and targeted drug delivery with different drug carriers to breast cancer cells have been investigated using the lab-on-a-chip device with the laser printed cellular patterns.

2. Materials and Methods

2.1 Chip design and fabrication

2.1.1 Computational fluid dynamics (CFD)-assisted chip design

The design of the proposed lab-on-a-chip device is shown in Fig. 1(A), and its dimensional design was optimized using a computational fluid dynamics (CFD) approach. The flow field in the upper channel of the designed chip was analyzed using CFD software (ANSYS FLUENT R16.0, ANSYS, Canonsburg, PA). As detailed in Supplementary Information (SI1), 3D models of the channel with realistic dimensions were created to simulate the flow field based on the optimized meshes and boundary conditions. The results from the simulation were post-processed in the software to assist the chip design.

2.1.2 Fabrication and preparation of the chip components

First, two polyethylene (glycol) diacrylate (PEGDA) molds (Fig. 1(B(i))) were fabricated using stereolithography (Supplementary Information SI2). Second, the chip lower and upper components, which are designed with channels and mounting holes, were fabricated using polydimethylsiloxane (PDMS) (Fig. 1(B(ii))). Silicone elastomer base and its curing agent

(Sylgard[®] 184, Dow Corning, Auburn, MI) mixed at a weight ratio of 10:1 were cast into the PEGDA-based molds, degassed for 2 hours at room temperature and then fully cured in an oven at 80°C for 1 hour. After curing fully, the PDMS components were peeled from the molds, respectively, and soaked in pure ethanol to wash away any residual PEGDA. Plexiglass slides (SIBE-R Plastic Supply, Ocala, FL) were cut and drilled for chip assembly and tubing was connected to the inlet and outlet holes with a biocompatible glue (Loctite 4011, Henkel, Düsseldorf, Germany). Porous polyester membrane (8 µm pore, Whatman, Sigma-Aldrich, St. Louis, MO) was cut to 40 mm × 20 mm to cover the channel, and the holes were punched for further assembly with the PDMS and plexiglass components.

2.1.3 Lab-on-a-chip system assembly

First, the lower plexiglass slide, lower PDMS component and porous membrane were aligned and bonded together to form the lower half of the chip after surface treatment with a laboratory corona treater (BD-20AC, Electro-Technic Products, Chicago, IL) as shown in Fig. 1(B(iii)). After sterilized with pure ethanol for 30 minutes and ultraviolet illumination for 10 minutes, the lower half of the chip was mounted onto a laser printing system²¹ as the deposition substrate onto which cellular patterns were printed as shown in Fig. 1(B(iv)). Then, the lower half of the chip was aligned and assembled with the sterilized upper PDMS component and upper plexiglass slide using screws to form a compact chip (Fig. 1(B(v))). To culture it under static conditions, the lower channel of the chip was filled with applicable cell culture medium and incubated in a humidified incubator with 5% CO₂ at 37°C. To introduce a pulsatile flow into the chip, the upper channel of the chip was connected with a cell culture medium reservoir via tubing, and the

medium was perfused using a peristaltic pump (Cole-Parmer, Vernon Hills, IL) as shown in Fig. 1(B(vi)) (Supplementary Information SI3).

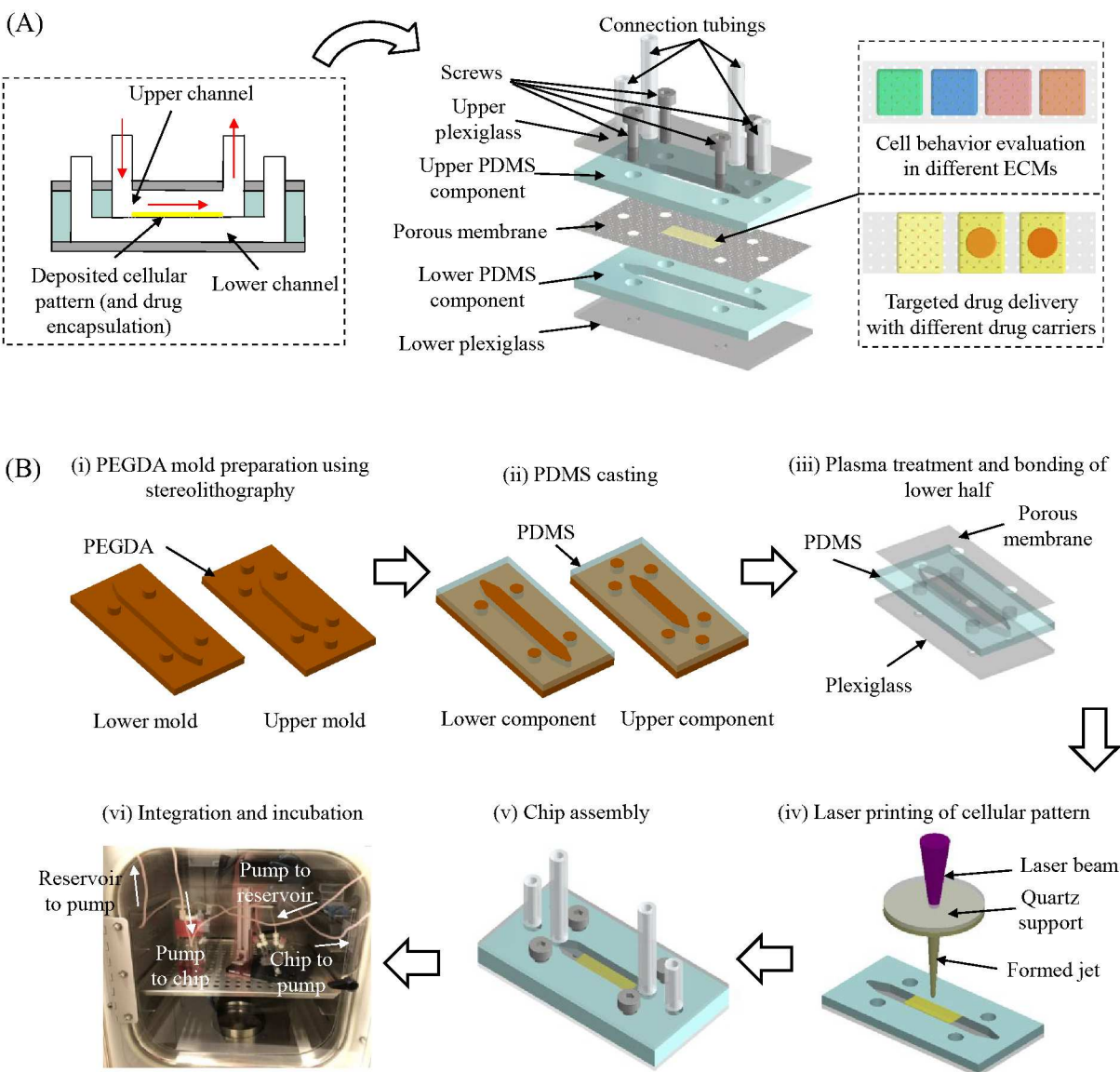


Fig. 1. (A) Design of the proposed lab-on-a-chip device. (B) Fabrication and use of the lab-on-a-chip device. (i) Fabrication of PEGDA molds using stereolithography. (ii) PDMS casting using the PEGDA molds. (iii) Plasma treatment of the lower plexiglass slide, lower PDMS component and porous membrane for bonding. (iv) Laser printing of cellular patterns on the bonded part from Step (iii). (v) Assembly of the bonded part with the upper PDMS component and upper plexiglass slide. (vi) Perfusion of the chip in the incubator with cell culture medium using a peristaltic pump.

2.2 Parallel evaluation of cellular behavior

2.2.1 Bioink preparation

As one of the most common components of ECM, collagen has been widely utilized to provide adhesion ligands for cultured cells. Collagen precursor solutions were prepared by diluting and neutralizing high concentration Type I rat tail collagen stock solutions (Corning, Manassas, VA) with 10× phosphate-buffered saline (PBS) (MP Biomedicals, Santa Ana, CA), sterilized DI water, and 1 mol/L sodium hydroxide (NaOH, Sigma-Aldrich, St. Louis, MO) in an ice bath to specified final collagen concentrations with a pH around 7.4. Sodium alginate (450–550 kDa, Acros Organics, NJ) was dissolved in cell culture medium as another component of cellular bioinks for its rapid gelation property upon interaction with calcium cations (Ca^{2+}). As a type of cells that synthesize structure framework in animal tissues and play a critical role in wound healing, fibroblasts were chosen to investigate the effect of ECM properties on cellular behavior, and NIH 3T3 mouse fibroblasts (ATCC, Rockville, MD) were cultured as previously described²¹. To prepare cell-laden bioinks, alginate and collagen solutions were mixed with fibroblast suspensions to result in four different bioinks containing 3.00 mg/mL collagen and 2.5×10^6 cells/mL fibroblasts, which were complemented with alginate at concentrations of 0% (no alginate), 0.25%, 0.50% and 1.00% (w/v), respectively.

2.2.2 Printing of cellular blocks on membrane

Laser-induced forward transfer printing²¹ was implemented herein to print different cellular blocks as detailed in Supplementary Information (SI4). To compare the morphology of fibroblasts under four different ECM formulations (collagen complemented with four different alginate concentrations), four cellular blocks were printed adjacently onto the polyester

membrane (Fig. 1(A)) using the four bioinks as prepared. For each block, four layers of a bioink were printed to create a cuboid approximately $3 \times 3 \times 0.2$ mm (L×W×H). For the blocks with alginate, an extra layer of 2% calcium chloride (CaCl_2 , Sigma-Aldrich, St. Louis, MO) was laser printed onto the top of each block to cross-link the alginate solution. Printed patterns were placed in a 37°C incubator for about 30 minutes for the collagen within each block to cross-link to form cell-laden gel patterns.

2.2.3 Measurement of cell viability

Immediately after cellular pattern printing, the cell viability in each region was measured using a trypan blue dye exclusion assay as introduced in Supplementary Information SI5. Briefly, the cell-laden gels were first liquefied using 0.055 mol/L sodium citrate (VWR, West Chester, PA) and 0.50% (w/v) collagenase (Sigma-Aldrich, St. Louis, MO) to release the cells. Then, the suspensions of dissociated cells were centrifuged to remove the supernatant, and the pellet was mixed with 0.4% trypan blue (Sigma-Aldrich, St. Louis, MO) to stain the dissociated cells. The cells were further loaded on a hemocytometer for observation using an optical microscope (EVOS XL, Grand Island, NY), the live and dead cells were counted to determine the cell viability.

2.2.4 Analysis of cell morphology

After 24 h or 72 h of culture under static or dynamic conditions, fluorescein diacetate (FDA) (Sigma-Aldrich, St. Louis, MO) was used to stain live cells within the cellular patterns on the designed chip and observe their morphology using fluorescence microscopy (EVOS FL, Grand Island, NY). The chip was first disassembled and the cell-laden hydrogel patterns were rinsed

with PBS and incubated in PBS containing 50 ng/mL FDA for 10 min at room temperature prior to imaging. Fluorescent images of the cells were captured to characterize and compare the morphology of the cells. In particular, two cell morphology parameters, circularity and aspect ratio, were measured from three independent experiments by outlining isolated cells with ImageJ (NIH, Bethesda, Maryland) for more than 50 cells per condition.

2.2.5 Characterization of ECM rheological properties

The mechanical properties of the collagen and alginate ECM formulations were characterized using an Anton Paar rheometer (MCR92, Anton Paar, Ashland, VA) with 25 mm diameter parallel plates. For test sample preparation, hydrogels containing collagen and alginate in required concentrations but without cells were cast in a 1 mm deep, 25 mm diameter mold. The alginate component was cross-linked with a nebulized 2% (w/v) CaCl_2 solution for 10 minutes and then the samples were placed in a 37 °C incubator for another 30 minutes to cross-link the collagen component. The gelled samples were carefully loaded onto the rheometer at 37 °C. For each gel formulation, a strain sweep from 0.01% to 1% strain was performed at a 1 Hz frequency to determine the linearly elastic regime. Then a frequency sweep was performed from 0.01 Hz to 1 Hz at a strain of 0.50% to measure the frequency-dependent storage modulus (G') of the gel as a function of frequency.

2.2.6 Characterization of diffusion coefficient

To analyze the efficiency of macromolecular transport within the gels used in this study, the diffusion coefficients of 70 kDa fluorescein isothiocyanate-dextran (FITC-dextran, Sigma-Aldrich, St. Louis, MO) in each gel formulation was determined following a well-established

protocol²³. For each hydrogel composed of collagen and/or alginate, 200 μL of its mixture containing 0.2 mg/mL FITC-dextran (total mass of 0.04 mg FITC-dextran) were transferred into a well in a standard 24-well plate and cross-linked by the same method as described above for the rheology specimens. Subsequently, 2 mL of PBS was slowly added to each well containing the gel. To satisfy the perfect-sink conditions and allow for the determination of the diffusion coefficient, 100 μL of the supernatant was collected into a standard 96-well plate at each time point after gently agitating the supernatant and replaced with the same volume of PBS. For the first 30 minutes, the supernatant was collected every 5 minutes, and then it was collected every 15 minutes until the last time point at 2 hours, resulting in 12 data points. The diffusion coefficient was calculated using the one-dimensional unsteady-state form of Fick's second law of diffusion, which is given as follows for small values of time (t)²⁴:

$$\frac{M_t}{M_\infty} = \left(\frac{16Dt}{\pi H^2} \right)^{1/2}$$

where D is the diffusion coefficient, M_t and M_∞ are the cumulative mass of the diffusing compound, FITC-dextran, released from the hydrogel at a given time point (t) and infinite time (∞), respectively. Herein, M_t was calculated based on the fluorescence intensity measured by a fluorescence plate reader (Synergy HT, Biotek, Winooski, VT) of the samples collected at each time point, and M_∞ was calculated based on the fluorescence intensity of 2 mL PBS containing 0.04 mg FITC-dextran, equivalent to the total amount of dextran that would be released into the supernatant. The gel thickness ($H=0.1$ cm) was calculated based on the volume of the gel and the dimensions of the well. D was obtained from the slope of the straight line fitting the data of M_t/M_∞ vs $t^{1/2}$ for $0 < M_t/M_\infty < 0.6$.

2.3 Targeted drug delivery to cancer cells

2.3.1 Bioink preparation

MCF-7 (ATCC, Rockville, MD), a widely utilized noninvasive breast cancer cell, were cultured in Minimum Essential Medium (MEM, Sigma-Aldrich, St. Louis, MO) supplemented with 10% fetal bovine serum (FBS, HyClone, Logan, UT), 5 $\mu\text{g}/\text{mL}$ insulin and 1% antibiotic-antimycotic solution in a humidified 5% CO_2 incubator at 37 $^\circ\text{C}$. The culture medium was replaced every 3 days. To collect cultured cells, freshly confluent flasks were washed twice with PBS and incubated with 0.25% trypsin/ethylenediaminetetraacetic acid (Sigma-Aldrich, St. Louis, MO) for 5 min at 37 $^\circ\text{C}$ to detach cells from the culture flasks. Then the cell suspension was centrifuged at 1000 rpm for 4 min at room temperature, and the resulting pellet was re-suspended in cell culture medium and mixed with a collagen solution to prepare a bioink containing 3.00 mg/mL collagen and 5×10^5 cells/mL MCF-7 cells.

2.3.2 Cell printing over drug encapsulations

Since sodium alginate has been widely adopted as drug carriers^{25,26}, it was utilized herein to encapsulate doxorubicin (DOX), a widely used anticancer drug, for controlled release to and treatment of surrounding MCF-7 cells. Doxorubicin hydrochloride (Sigma-Aldrich, St. Louis, MO), was first dissolved in PBS and then mixed with sodium alginate to form two formulations with concentrations of 0.50% (w/v) or 1.00% (w/v) sodium alginate with 500 $\mu\text{g}/\text{mL}$ DOX. In order to encapsulate DOX, two alginate-based cylindrical depots about 2 mm diameter and 0.2 mm high were printed using the two alginate-DOX mixtures and cross-linked by printing another layer of 2% CaCl_2 solution over them. After that, four layers of the MCF-7 cell-laden bioink were printed to generate two $4 \times 3 \times 0.2$ mm (Length \times Width \times Height) blocks with the same

amount of living cells, completely covering the two drug encapsulations, respectively. For comparison, another independent block with the same dimensions containing the same amount of living cells was also printed on the designed chip as the no-direct drug delivery control using the same bioink. The whole structure was placed in a 37 °C incubator for about 30 minutes for the collagen precursor to gel.

Assuming all DOX in the two encapsulations are released into the cell culture medium utilized in the system after infinite time, the final DOX concentration is 16 ng/mL. Therefore, the cell culture medium with this DOX concentration was also prepared to culture the equivalent MCF-7-laden collagen gel under static culturing conditions as a control to investigate whether the total amount of DOX released into the system has any effect on the cancer cells.

2.3.3 Characterization of cell viability and diffusion coefficient

After one day of incubation, the cell viability of the MCF-7 cells cultured with different drug carriers were measured with the dye exclusion assay as aforementioned. To analyze the drug release rate from the two drug formulations, the diffusion coefficients of 70 kDa FITC-dextran through the alginate gels with 0.50% and 1.00% concentrations, respectively, was determined by following the same protocol as previously used²³.

2.4 Statistical analysis

All cell-related measurements were obtained from at least three independent repeats. Cell morphology parameters including the circularity and aspect ratio were reported as the boxplot displaying the mean, median, quartiles, 5th percentile and 95th percentile of the data. Evaluation

of the difference between the mean values of each group was performed by Student's *t*-test, in which a *p* value of $p < 0.05$ was considered significant.

3 Results and discussion

3.1 Design of the lab-on-a-chip system

To mimic the *in vivo* biological environment with living cells supported by both blood and interstitial flows, the chip (Fig. 2(A)) was designed with two adjacent PDMS-based channels separated by a thin porous polyester membrane (~10 μm thickness) on which the cellular patterns (and drug encapsulations) were printed. The two pieces of plexiglass were designed to help seal the whole chip and provide the interfaces with the perfusion tubes. Plasma treatment, a typically utilized method to seal a PDMS-based chip, may injure cells after a cellular pattern was printed, so assembly holes were designed on the chip and all the parts were clamped together by screws. As illustrated in Figs. 1(A) and 2(B), the upper channel was designed to connect with the peristaltic pump to introduce a pulsatile flow of cell culture medium. The lower channel was designed to be filled with a static cell culture medium to mimic the interstitial space. Also, a physiologically relevant interstitial flow through the cellular patterns and porous membrane was made possible due to the diffusion of cell culture medium between the upper and lower channels. The cell culture medium in the lower channel was refreshed by a syringe or pipette as required through two connectors with the lower channel.

The patterns in the designed chip are created using the laser printing method. Laser printing of a pattern is mainly consisted of three processes, namely jet formation, droplet deposition, and automatic control processes. Jet formation is the process in which a jet is formed due to the

converted kinetic energy from the laser-matter interaction process between the laser pulse and printing material on the quartz support. The morphology of a formed jet may vary from no material transferring to well-defined jetting to well-defined jetting with an initial bulgy shape to jetting with a bulgy shape to pluming/splashing with different printing conditions and materials²⁷. In particular, jet formation process with well-defined jetting is desirable for high quality laser printing. After the jet is formed, it may or may not break up into droplets before depositing on a printing substrate in the droplet deposition process. Depending on printing conditions and material properties, there are three different droplet deposition processes: droplet-impingement printing, jet-impingement printing with multiple breakups, and jet-impingement printing with a single breakup³⁴. These three different droplet deposition processes result in different morphologies of deposited droplets. To form a required pattern with automatic control²⁹ of the printing system, the formed droplets are deposited in a layer-by-layer fashion. Process control affects the morphology of formed patterns and layer formation process and further determines the quality of printed structures^{21, 30}. Furthermore, process-related parameters, such as the laser fluence, laser spot size and direct-writing height (i.e., ink ribbon and printing substrate distance), affect the aforementioned jet formation and droplet deposition processes. Besides the laser fluence, the laser spot size directly determines the size of formed bubbles after the laser-matter interaction process^{31, 32}. As a result, it affects the sequential jet formation and droplet deposition processes and finally the morphology and size of each deposited droplet. Direct-writing height affects the droplet/jet landing and impingement processes during droplet deposition. By adjusting the direct-writing height, the droplet deposition process may change from droplet-impingement printing to jet-impingement printing with multiple breakups to jet-impingement printing with single breakup²¹. Printing material properties, such as the viscosity

and surface tension, are also of importance in determining the printing quality. The viscosity of printing materials affects both the jet formation and droplet deposition processes²¹ and therefore the size and morphology of deposited droplets. Surface tension of printing materials affects the uniformity of ink coating on the quartz support and therefore the consistency in the morphology and size between forming droplets. It may also affect the coalescence process of two adjacently deposited droplets. Specifically, the printability of cell-laden bioinks can be mapped in the same two Weber-Ohnesorge and Weber-elasto-capillary phase diagrams as during the laser printing of non-Newtonian fluids. The effects of cell media and living cells on the bioink printability can be sufficiently captured by the material property-related Ohnesorge and elastocapillary numbers³³.

As the jet formation and droplet deposition processes are of importance and depend on the printing conditions and material properties, the applicable laser fluence for each cellular bioink was identified based on the observed jet formation and droplet deposition processes (Supplementary Information SI4). Fig. 2(C) shows some representative images of the jet/droplet formation and impingement process of the cellular bioink containing 1.00% alginate, 3.00 mg/mL collagen and 2.5×10^6 cells/mL fibroblasts, which was printed using an applicable laser fluence of 600 mJ/cm². More detailed information about the jet/droplet formation and impingement process are included as Supplementary Information SI4. Due to the effect of living cells on the printing process, the printing type³⁴ in this study is classified as droplet-impingement printing for bioinks without alginate and jet-impingement printing with multiple breakups for bioinks with alginate. Each printed bioink turned to be a cell-laden ECM gel after cross-linking.

The printing resolution herein, defined as the minimum size of printed features herein, is mainly determined by the size of each single droplet deposited on a printing substrate. The resolution is mainly determined by the laser spot size (influencing the laser-matter interaction and bubble formation processes), printing conditions and bioink rheological properties (influencing the droplet formation and deposition processes), and cell concentration. In particular, the laser spot size affects the size of formed bubbles after the laser-matter interaction process^{31, 32} and therefore the final size of each formed droplet. During the droplet deposition process, the resulting printing morphology/pattern can be multiple randomly distributed droplets, one main droplet with satellite droplet(s) or one main droplet³⁴. In terms of the printing quality, the morphology of one main droplet is most desirable as the location and distribution of deposited droplets during printing is the most controllable. When printing with cell-laden bioinks, non-straight jets may form due to the effect of randomly distributed living cells³³. As a result, the most desirable morphology of deposited droplets (one main droplet) may not always be achievable during the printing of cellular patterns. In this study, the printing resolution in terms of the droplet size can be achieved approximately 200 μm by optimizing printing conditions for a given bioink, and this can be further improved by updating the laser beam delivery system for smaller laser spot sizes. With the feasibility to create various micro-patterns in high efficiency, theoretically speaking, laser printing can be utilized to create a large amount of patterns for testing in lab-on-a-chip devices. As shown in Fig. 2(D), 10×10 microarrays of alginate are efficiently printed on a glass slide in high shape fidelity. Due to the design requirements (channel dimensions) in this study, the feasibility of laser printing in creating a large amount of testing patterns in lab-on-a-chip devices is not specifically demonstrated.

To lessen the direct impact from the inlet and outlet perfusion flows, two 2.5 mm long transition zones were included at both the inlet and outlet in the upper channel along the horizontal direction. Excluding the transition portions, the upper channel was designed with a length of 15 mm, and the width and height was designed to be 4×3 mm (W×H) based on CFD simulations. A suitable average flow rate in the upper channel is determined as 2.5 mL/min. This results in an average flow velocity of 10 mm/s approximately in the upper channel, as shown in simulated stream lines in Fig. 2(D), which is in the range of blood flow velocity in human body³⁵. Based on the estimated Reynolds number (~ 1) from the CFD simulation is, the fluid flow in the designed channel is laminar (Supplementary Information SI1). The total pressure distribution on the bottom of the upper channel, where the cells were printed and cultured, was also analyzed using CFD and a uniform total pressure distribution was confirmed (Supplementary Information SI1). That is, the local pressure experienced by cells within the chip is independent of its location, indicating that the experimental conclusions are not location dependent in the chip. Depending on whether the upper channel is connected or not with the peristaltic pump during testing, the testing condition is defined as dynamic or static culturing, respectively.

Once the upper channel was designed, the lower channel, which served as a reservoir of static cell culture medium, was designed correspondingly with a total length of 32 mm, width of 4 mm, and height of 3 mm. Based on the above design, the whole chip is shown in Fig. 2(E).

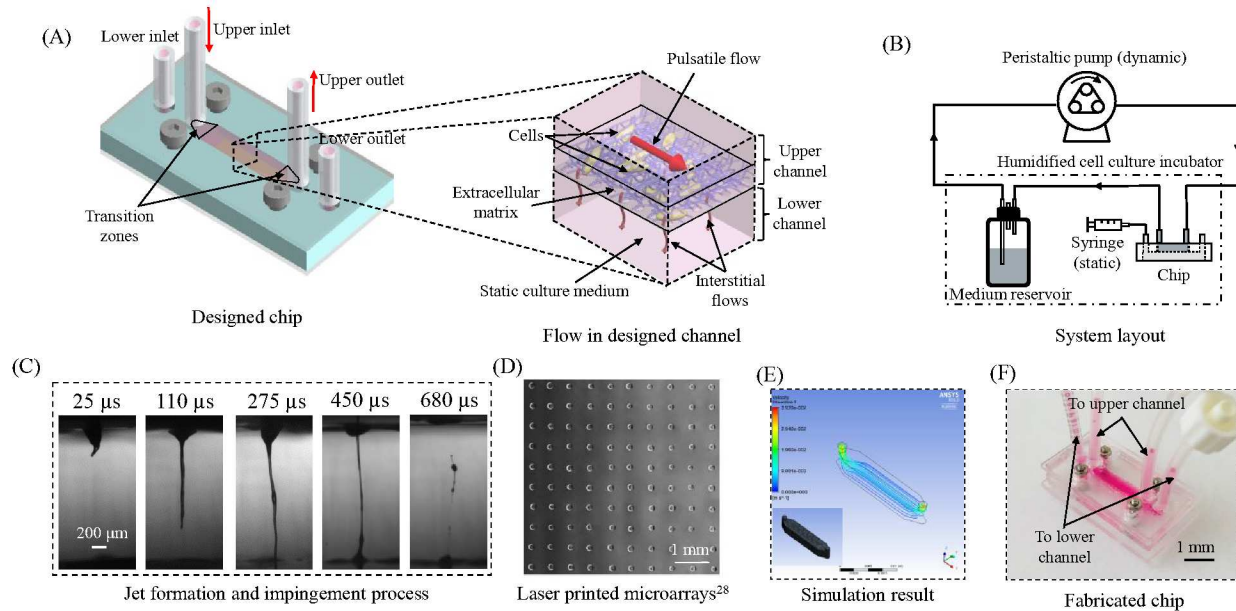


Fig. 2. (A) Schematic of the designed chip with the pulsatile and interstitial flows, (B) layout of the whole lab-on-a-chip system, (C) representative images of the jet formation and impingement process during laser printing of a bioink (1.00% alginate, 3mg/mL collagen and 2.5×10^6 cells/mL fibroblasts) at 600 mJ/cm^2 , (D) microarrays printed from 8% alginate on a glass slide (Reprinted with permission from American Chemical Society), (E) CFD simulated streamline in the upper channel, and (F) the fabricated chip filled with cell culture medium.

3.2 Parallel evaluation of cellular behavior

Laser printing in the designed lab-on-a-chip device enables the creation of heterogeneous physical, chemical, and biological cues for living cells cultured in the designed lab-on-a-chip device. As one application, parallel evaluation of cellular behavior under varied physical and chemical culturing conditions in a biomimetic physiological environment is demonstrated in terms of the effects of ECM properties on the cell morphology.

3.2.1 Cellular pattern creation with varying ECM formulations

As illustrated in Fig. 3(A), four adjacent cellular blocks were printed in the designed chip to evaluate the proliferation behavior of cells cultured in different ECM environments from four cellular bioinks. The cell viability in the four cellular patterns immediately after printing were above 90% as shown in Fig. S4 of Supplementary Information (SI5) which confirms the feasibility of using laser bioprinting in creating living cellular patterns for further culturing and biological investigations. It is noted that the cell viability after printing is higher than those printed in a previous study²¹, and it is attributed to the shorter printing time and milder gelation process in this study.

Under dynamic culturing conditions, the flow rate of the peristaltic pump was 2.5 mL/min. The relative position of the inlet and outlet during dynamic culturing was changed between each repeat to prove that the experimental observation is not dependent on the location of cellular patterns in the chip herein. After the printed cellular patterns were incubated for 24 h or 72 h under dynamic and static conditions, respectively, cells in the different cellular patterns show different morphologies in responding to different ECM properties (different alginate percentages) and culturing conditions (different flow conditions). Representative images of cells cultured in different patterns with different culturing time and culturing conditions are shown in Fig. 3(B). Under different conditions, fibroblasts may spread out and exhibit the elongated, spindle-like morphology such as in 3.00 mg/mL collagen after 72 h of dynamic culturing while some may remain spherical, with very little extension or spreading visible such as in 1.00% alginate and 3.00 mg/mL collagen after 24 h of static culturing.

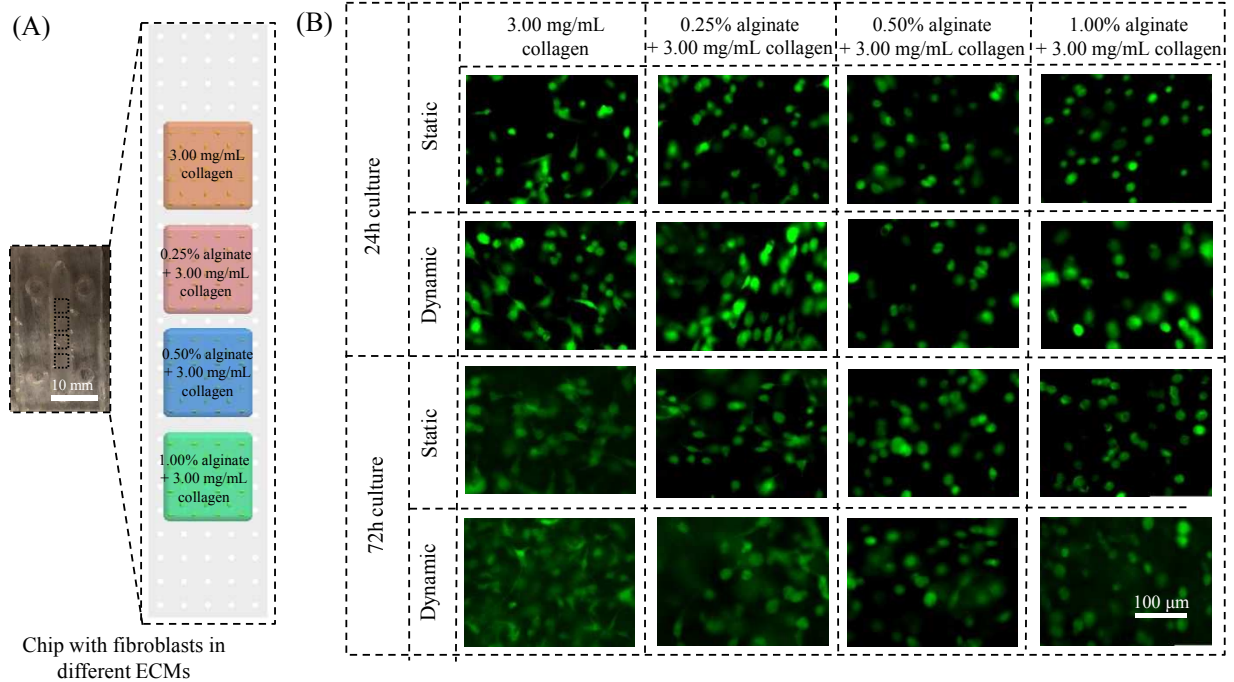


Fig. 3. (A) Schematic illustration of the layout of four cellular patterns and images of printed cellular patterns in the chip, and (B) representative fluorescent images of cells cultured under different conditions.

3.2.2 Quantitative characterization of cell morphology

Circularity and aspect ratio of living cells were calculated and utilized together to quantitatively assess the morphology difference of cells cultured under different conditions. Circularity ($4\pi \times \text{area} / \text{perimeter}^2$) describes the roundness of a cell and ranges from 0 to 1, with 1 denoting cells with a perfectly circular shape. Aspect ratio (major axis/minor axis of the best-fit ellipse) describes the elongation of a cell and is larger than 1, and an increasing value denotes a cell with more polarization. Generally, the calculated circularity and aspect ratio of observed cells are distributed between two regimes: 1) rounded with high circularity and low aspect ratio (Fig.

4(A), panels i & ii) which indicates low cell spreading, and 2) elongated with low circularity and high aspect ratio (Fig. 4(A), panels iii & iv) which indicates well spreading. Average circularity and aspect ratio of cells cultured under different conditions are presented in Fig. 4(B). Under the same incubation time and culturing conditions, cells embedded within ECM with lower alginate concentrations exhibit better spreading with lower circularity and higher aspect ratio. Hydrogels with higher alginate concentrations inhibit cell spreading, and cells embedded within such hydrogels exhibit larger circularity and lower aspect ratio. After 72 h of incubation, cells embedded in a given ECM formulation spread more and exhibit a relatively smaller circularity and larger aspect ratio than that after 24 h incubation. In addition, it is found that at a given time point, cells exhibit a smaller circularity and larger aspect ratio when cultured under dynamic conditions than those when cultured under static conditions in the same ECM formulation.

3.2.3 Analysis of hydrogel properties and culturing conditions

As the same amount of collagen was utilized herein in each bioink, cells in each ECM gel were presented with the same concentration of adhesion ligands. Since alginate does not provide adhesion ligands for cells, the variation in morphology of cells embedded in different ECM gels is not due to the variation in the amount of adhesion ligands herein. As such, the effect of molecular composition on the cellular behavior is negligible.

The ECM gels in this study have different mechanical properties due to the different amount of alginate. To characterize the mechanical properties of each ECM gel, rheological testing was performed. The frequency-dependent storage modulus (G') of each gel measured at a strain of 0.50% is shown in Fig. 4(C), and the strain sweep can be seen from Supplementary Information

SI6. The gels with a higher alginate concentration exhibit higher storage moduli, indicating higher stiffness of ECM gel for embedded cells. Cells probe the mechanical properties of their microenvironment and dynamically re-organize their cytoskeleton in response to the resistance they detect⁴². For formulations with low mechanical stiffness in 3D cell culture, the gel resistance to cellular re-organization is relatively low enough to allow cells to spread, contract, and invade the surrounding gel. Therefore, stiffer ECM may inhibit cell spreading, and softer ECM is preferred for cells to spread out under given culturing conditions.

Besides molecular composition and ECM stiffness, the mass transport behavior, characterized using the diffusion coefficient, of a gel is crucial for cells as diffusion within ECM gels directly influences the local microenvironment that supplies cells with necessary nutrients and oxygen^{42,43}. Because of this, the diffusion coefficient of different ECM gels was characterized (1.0×10^{-7} cm²/s for collagen only and 5.3×10^{-10} , 2.0×10^{-10} , and 4.8×10^{-11} cm²/s for collagen with 0.25%, 0.50% and 1.00% alginate, respectively) by using FITC-dextran (70 kDa) as shown in Fig. 4(D) (Supplementary Information SI7). As observed, the higher the concentration of alginate, the lower the diffusion coefficient of the formed gel. This may be attributed to the higher chain density and entanglement of gels with a higher alginate concentration³⁹. Since higher diffusion coefficients indicate rapid diffusion which effectively facilitates the nutrient supply, oxygen diffusion, and metabolic waste removal, cells embedded in ECM gels with higher diffusion coefficients may be more active as demonstrated by aggressive adhesion and spreading. As such, cells in ECM gels with a low alginate concentration exhibit better spreading.

Compared with static culturing, dynamic culturing promotes cell spreading in a given ECM as characterized by the cell circularity and aspect ratio. This is consistent with other observations such as 3D cultured human mesenchymal stem cells⁴⁰. On the one hand, convection of cell culture medium on the cellular patterns due to the pulsatile flow in the upper channel facilitates both nutrient supply to the cells and removal of metabolic waste from the cells, which may enhance the metabolic activity of the cells and therefore facilitate cell spreading. On the other hand, the pulsatile flow in the upper channel promotes the interstitial flow between the upper and lower channels through the printed cellular patterns. Mechanotransduction studies have shown that interstitial flow-induced shear stress increases the secretion of matrix metalloproteinases (MMPs) in fibroblasts⁴¹. As MMPs are endopeptidases related to invading or remodeling the extracellular microenvironment^{36,37}, with a higher MMP activity, cell spreading within a certain ECM may be promoted.

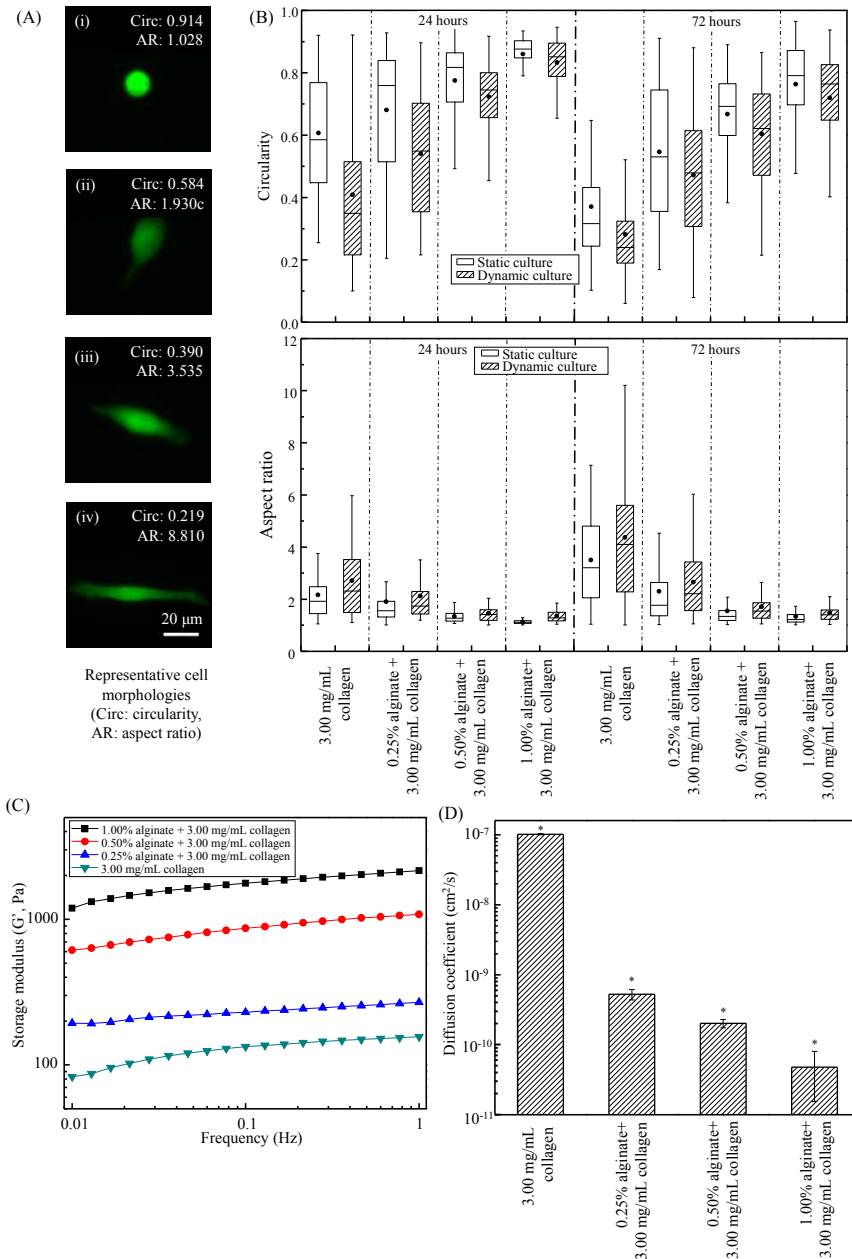


Fig. 4. (A) Representative images of cells with different circularity (Circ) and aspect ratio (AR). (B) Boxplot of calculated circularity and aspect ratio of cells cultured under different conditions (More than 50 cells per condition were calculated from three independent experiments). Statistically significant difference of average value was found when comparing different ECMs with a given set of incubation time and culturing conditions, different culturing conditions with a given set of ECM and incubation time conditions, different incubation times with a given set of ECM and culturing conditions, and different culturing conditions with a given set of ECM and incubation time conditions. (C) Representative results of characterized storage modulus of different ECM gels. (D) Measured diffusion coefficient of different gels (error bar indicates \pm standard deviation, * indicates statistical difference between each other with $p < 0.05$, and $n = 3$).

3.2.4 Assessment of scaffold materials and culturing conditions for cell printing

The cultured fibroblasts with low circularity, high aspect ratio morphology show good replication of the *in vivo* fibroblast spindle morphology as reported before⁴⁴. Therefore, ECM and culturing conditions which facilitate the spreading and elongation of fibroblasts are preferred for the fibroblasts herein. As aforementioned, fibroblasts exhibit very weak spreading in the ECM with a high alginate concentration since the ECM is too stiff even if enough adhesion ligands are provided. Broadly speaking, the results suggest that for a hydrogel to be a good bioink material in cell printing, it is important to modulate both its molecular composition (i.e. amount of binding sites) and mechanical properties (i.e. matrix stiffness) for the successful recapitulation of *in vivo* behavior of living cells. Hydrogels with very high stiffness may be preferred during printing in order to increase the printing quality and shape fidelity of printed constructs, however, they may hinder the spreading and other behaviors of cells cultured within the printed constructs. The four bioinks utilized herein can be substituted by any other biomaterials and cells and printed in the designed chip with the same method to investigate the feasibility or optimize the formulation of certain materials to serve as bioink materials in cell printing. Also, as can be seen from the above results, dynamic culturing conditions may promote spreading and other related behavior of cells in printed cellular patterns compared to those under static culturing conditions. Culturing conditions mimicking the *in vivo* physiological environment may be more efficient in promoting functional maturation of printed cellular structures.

3.3 Targeted drug delivery to cancer cells

Directly printing cellular patterns in a designed chip also enables the fabrication of hybrid cellular and acellular patterns to fulfil certain testing requirements. Therefore, targeted drug delivery is demonstrated as another application herein. Specifically, the effects of different drug carriers on the chemotherapeutic drug delivery to breast cancer cells are investigated in the designed chip.

3.3.1 Printing drug-encapsulated cellular patterns

Three different cellular patterns were printed as shown in Fig. 5(A): two $4 \times 3 \times 0.2$ mm cellular patterns containing the same amount of living cells each with an encapsulated drug depot containing the same amount of anticancer drug DOX but in two different drug carriers (0.50% (w/v) and 1.00% (w/v) alginate), respectively, and one pure cellular pattern at the same size and containing the same amount of living cells as the no-direct DOX delivery control. All the cell patterns were cultured under dynamic conditions to better mimic *in vivo* physiological conditions with a flow rate of 2.5 mL/min. It should be noted that different droplet sizes were generated when printing these two drug depots due to the difference in alginate concentrations. By adjusting the printing speed, the two alginate-based drug depots have approximately the same volume and therefore contain the same mass of active drug. The MCF-7 cell and collagen bioink printed over the drug depots are utilized to mimic the *in vivo* situation of cancer cells treated with directly released anticancer drugs. The no-direct DOX delivery pattern was away from the drug depots but still able to interact with the drug released into the culture environment.

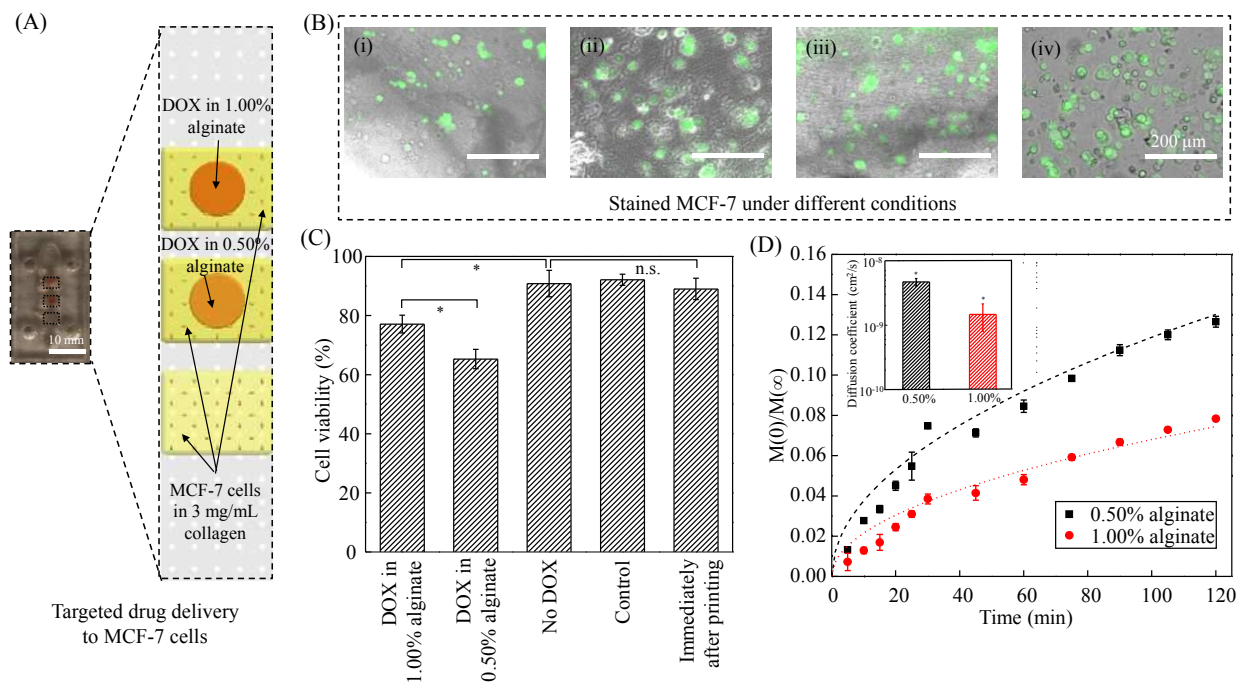


Fig. 5. (A) Image and schematic illustration of MCF-7 cellular patterns encapsulated with drug depots. (B) Images of cells cultured under different conditions: (i) DOX in 1.00% alginate, (ii) DOX in 0.50% alginate, (iii) no DOX, and (iv) control. (C) Cell viability under different conditions. (D) Characterized drug release process with FITC-dextran and calculated diffusion coefficient (Error bar indicates \pm one standard deviation, and * indicate the statistical difference between each other with $p < 0.05$, $n = 3$).

3.3.2 Cell viability under different drug delivery conditions

After 24 h of incubation, cells cultured under different drug delivery conditions were observed, and their viability was tested. The FDA-stained MCF-7 cells cultured under different conditions are shown in Fig. 5(B) with stacked fluorescent and phase contrast images, and the viability of cells cultured under different drug delivery conditions is shown in Fig. 5(C). Cells with targeted DOX delivery from the lower concentration alginate (0.50%) exhibit lower viability with the

average viability of 65.3 % which is significantly lower than the 77.1% viability of cells with targeted DOX delivery from the higher concentration (1.00%) alginate encapsulation. This indicates the effect of different drug carriers on the chemotherapy effectiveness on cancer cells. It is also shown that cells cultured in the chip without targeted DOX delivery (the no-direct DOX delivery pattern) exhibit the viability around 90% and the viability of cells of the static culturing control group is also around 90%. There is no statistical difference in terms of the cell viability among the no-direct DOX delivery pattern, the statically cultured control, and the cells immediately after printing, indicating no significant effect of the anticancer drug without targeted delivery.

3.3.3 Characterization of drug release process

To assess the drug release rate in the two alginate encapsulations, the release process of FITC-dextran (70 kDa) from the gels created using 1.00% and 0.50% alginate was observed and characterized to determine the difference in drug release rate. The modeled drug release process of dextran in 2 hours and characterized diffusion coefficient of each alginate gel are shown in Fig. 5(D) (4.6×10^{-9} cm²/s for 1.00% alginate and 1.5×10^{-9} cm²/s for 0.50% alginate). The results indicate that at a given time point, more dextran is released by 0.50% alginate gel than by 1.00% alginate gel, indicating a higher drug release rate from low concentration alginate gels. It should be noted that since dextran is a macromolecule with a much higher molecular weight (70 kDa) than DOX (544 Da), and the condition under which the dextran release process was characterized is different from the real condition under which DOX was released in the designed chip, the measured results herein can only provide a qualitative analysis of the DOX release process from the two encapsulations adopted in the chip. The results show that DOX delivered

from the less concentrated alginate gel is released more rapidly to its surrounding during the first 24 h so that cells cultured around the DOX encapsulation are subjected to a higher local dosage of DOX at a given time, resulting in the relatively lower viability of cells cultured with the 0.50% alginate DOX targeted drug delivery depot.

3.3.4 Effect of drug delivery conditions

The above result shows that without direct targeted delivery of anticancer drugs, effective chemotherapy on cancer cells might be difficult to be achieved as cells cultured in the chip without directly delivered DOX and in the statically cultured control group show no significant decrease in the cell viability. This indirectly implies the importance of targeted drug delivery, which is also confirmed by a previous study which showed that DOX treatment using tumor-targeted drug carriers *in vivo* is significantly more effective than free DOX for destroying tumors⁴⁵. Drug release rate is also an important factor which affects the chemotherapy to cancer cells as our results show that drug carriers with different drug release rates result in different chemotherapy effects on cancer cells under a given set of conditions. The designed chip with the laser-printed cellular patterns herein can be further utilized to investigate the chemotherapeutic effect of other drugs on specific cells or tissues as an efficient tool for drug screening and other related investigations.

3.4 Advantage of laser printing in creating biological patterns

To create biological patterns (mainly, cellular) for functional testing on a designed chip, there are three typically utilized methods: photolithography, contact printing (also called stamping⁴⁶) and microfluidic patterning. The comparisons of these three methods with the LIFT-based printing

method are listed in Table S2 (Supplementary Information SI8) in terms of the material compatibility, geometric feasibility and process complexity. In photolithography, designed patterns, containing cell-adhesion materials for cell seeding, are generally created using ultraviolet (UV) light, photoresist and mask. Although it is very convenient to create customized patterns using photolithography, most chemicals used in photolithography are toxic to cells and may denature biomolecules⁴⁶, limiting its applications for creating biological patterns in lab-on-a-chip devices. Contact printing/patterning is developed based on the contact transfer of materials of interest from an elastomeric stamp onto a certain surface area contacted by the stamp. Although this method has been widely utilized to create biological patterns with proteins⁴⁷ and cells⁴⁸, its main limitation is to create patterns with three or more different types of materials^{49, 50} and multi-layered testing patterns. Microfluidic patterning utilizes pre-created channels to selectively deliver cells and biomaterials to certain areas on a substrate to form biological patterns^{9, 10, 13, 14}. Although it is easier to create patterns with many different materials when compared to photolithography and contact printing/stamping⁵⁰, it is limited in creating patterns without open network geometries⁵¹. Also, it may be hard to pattern high viscosity materials with microfluidic patterning due their low fluidity.

As an innovative orifice-free 3D printing method, LIFT is capable of creating any biological/cellular patterns^{22, 52, 53} in lab-on-a-chip devices. It can be utilized to directly transfer cells and biomaterials to form customized patterns without the pre-processing and additional cell seeding steps as required in photolithography. Due to its orifice-free 3D printing nature, highly viscous materials can be easily printed using LIFT, and different materials can be easily patterned onto the same surface by simply switching quartz supports coated with corresponding

materials. It is also very easy to create multi-layered structures in lab-on-a-chip devices by following a layer-by-layer fashion as introduced before²¹. As compared with these typical cell patterning methods, LIFT-based printing has two main advantages in creating biological patterns in lab-on-a-chip devices: high efficiency in directly creating biological patterns without pre-processing and additional cell seeding needs and high versatility in producing 3D customizable multi-layered patterns from a variety of materials.

4 Conclusions and future work

Laser printing is a versatile technique capable of creating patterns integrating cells and biomaterials. Herein, laser printing has been adopted to develop a new method of directly creating multiple customized heterogeneous cellular patterns for cell-related testing in a lab-on-a-chip device. This method can improve the efficiency and versatility of cell-related testing and evaluation applications with lab-on-a-chip devices. As application demonstrations, parallel evaluation of cell behavior within different ECMs and assessment of different drug carriers on the effectiveness of targeted drug delivery to cancer cells have been investigated and characterized using the proposed lab-on-a-chip device. ECM formulations with lower stiffness and dynamic culturing conditions effectively promote cell spreading and proliferation. Targeted drug delivery is proved important for effective chemotherapy and drug release rate of drug carriers affects the chemotherapy to cancer cells. For the wide implementation of this new method, some future work is proposed as follows. First, more functionally relevant lab-on-a-chip devices are to be created with this advanced fabrication-based method to enhance the versatility of lab-on-a-chip devices in simulating tissue- and organ-level physiology. Second, designed chip

integrated with in-line sensors about critical functional parameters (e.g., flow rate, pressure, temperature, pH, oxygen concentration) capable to monitor overall system performance is to be developed using the proposed fabrication method for better cell-related sensing and evaluation applications. Third, lab-on-a-chip devices will be designed to accommodate a large amount of cellular patterns which can be effectively fabricated using laser printing.

Acknowledgements

This research was partially supported by NSF (CMMI-1537956) and the Florida Breast Cancer Foundation, and the access of the Anton Paar rheometer at the University of Florida and Kaidong Song's assistance are appreciated.

References

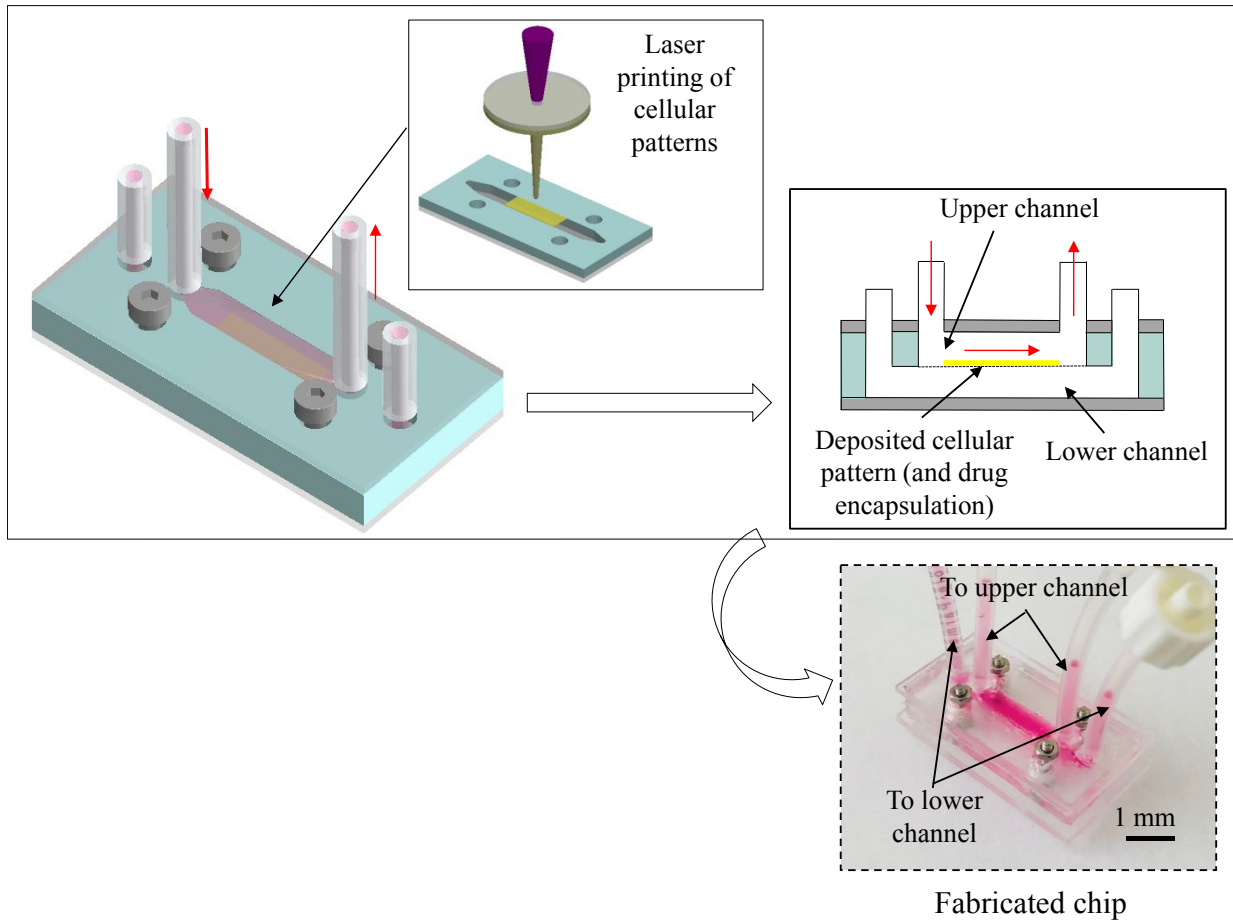
1. K. Yum, S. G. Hong, K. E. Healy and L. P. Lee, *Biotechnol. J.*, 2014, 9, 16-27.
2. D. Huh, Y. S. Torisawa, G. A. Hamilton, H. J. Kim and D. E. Ingber, *Lab on a Chip*, 2012, 12, 2156-2164.
3. S. N. Bhatia and D. E. Ingber, *Nature Biotechnol.*, 2014, 32, 760-772.
4. J. El-Ali, P. K. Sorger and K. F. Jensen, *Nature*, 2006, 442, 403-411.
5. J. D. Caplin, N. G. Granados, M. R. James, R. Montazami and N. Hashemi, *Adv. Healthc. Mater.*, 2015, 4, 1426-1450.
6. K. J. Jang, A. P. Mehr, G. A. Hamilton, L. A. McPartlin, S. Chung, K. Y. Suh and D. E. Ingber, *Integr. Biol.*, 2013, 5, 1119-1129.
7. Y. S. Torisawa, C. S. Spina, T. Mammoto, A. Mammoto, J. C. Weaver, T. Tat and D. E. Ingber, *Nat. Methods*, 2014, 11, 663.

8. F. Gioiella, F. Urciuolo, G. Imparato, V. Brancato and P. A. Netti, *Adv. Healthc. Mater.*, 2016, 5, 3074-3084.
9. P. J. Lee, P. J. Hung and L. P. Lee, *Biotechnol. Bioeng.*, 2007, 97, 1340-1346.
10. J. S. Jeon, I. K. Zervantonakis, S. Chung, R. D. Kamm and J. L. Charest, *PloS one*, 2013, 8, e56910.
12. L. Wang, J. Zhu, C. Deng, W. L. Xing and J. Cheng, *Lab on a Chip*, 2008, 8, 872-878.
13. J. H. Sung and M. L. Shuler, *Lab on a Chip*, 2009, 9, 1385-1394.
14. J. H. Sung, C. Kam and M. L. Shuler, *Lab on a Chip*, 2010 10, 446-455.
15. L. Zhao, T. Guo, L. Wang, Y. Liu, G. Chen, H. Zhou and M. Zhang, *Anal. Chem.*, 2017, 90, 777-784.
16. L. Moroni, J. R. De Wijn and C. A. Van Blitterswijk, *Biomaterials*, 2006, 27, 974-985.
17. K. Jakab, C. Norotte, F. Marga, K. Murphy, G. Vunjak-Novakovic and G. Forgacs, *Biofabrication*, 2010, 2, 022001.
18. Y. Huang and S. R. Schmid, *ASME J. Manuf. Sci. Eng.*, 2018, 140, 094001.
19. A. I. Shallan, P. Smejkal, M. Corban, R. M. Guijt and M. C. Breadmore, *Anal. Chem.*, 2014, 86, 3124-3130.
20. L. E. Bertassoni, M. Cecconi, V. Manoharan, M. Nikkhah, J. Hjortnaes, A. L. Cristino and A. Khademhosseini, *Lab on a Chip*, 2014, 14, 2202-2211.
21. R. Xiong, Z. Zhang, W. Chai, Y. Huang and D. B. Chrisey, *Biofabrication*, 2015, 7, 045011.
22. R. Xiong, Z. Zhang, W. Chai, D. B. Chrisey and Y. Huang, *Biofabrication*, 2017, 9, 024103.
23. S. Koutsopoulos, L. D. Unsworth, Y. Nagai and S. Zhang, *Proc. Natl. Acad. Sci.*, 2009, 106, 4623-4628.
24. J. Crank and G. S. Park, *Diffusion in Polymers*, 1968, London and New York.

25. M. Rajaonarivony, C. Vauthier, G. Couarraze, F. Puisieux, and P. Couvreur, *J. Pharm. Sci.*, 1993, 82, 912-917.
26. M. George and T. E. Abraham, *J. Control. Release*, 2006, 114, 1-14.
27. Z. Zhang, R. Xiong, R. Mei, Y. Huang, and D. B. Chrisey, *Langmuir*, 2015, 31, 6447-6456.
28. Z. Zhang, C. Xu, R. Xiong, D. B. Chrisey and Y. Huang, *Biomicrofluidics*, 2017, 11, 034120.
29. H. Gudapati, J. Yan, Y. Huang, and D. B. Chrisey, *Biofabrication*, 2014, 6, 035022.
30. R. Xiong, Z. Zhang, and Y. Huang, *J. Manuf. Process.*, 2015, 20, 450-455.
31. W. Wang, G. Li, and Y. Huang, *J. Manuf. Sci. Eng.*, 2009, 131, 051013.
32. Z. Zhang, Y. Jin, J. Yin, C. Xu, R. Xiong, K. Christensen, B. R. Ringeisen, D. B. Chrisey, and Y. Huang, *Appl. Phys. Rev.*, 2018, 5, 041304-1-21.
33. M. S. Brown, N. T. Kattamis, and C. B. Arnold, *J. Appl. Phys.*, 2010, 107, 083103.
34. Z. Zhang, R. Xiong, D. T. Corr and Y. Huang, *Langmuir*, 2016, 32, 3004-3014.
35. E. N. Marieb and K. Hoehn, *Human Anatomy & Physiology*, 2007, Pearson Education.
36. D. E. Discher, P. Janmey and Y. L. Wang, *Science*, 2005, 310, 1139-1143.
37. J. L. Drury and D. J. Mooney, *Biomaterials*, 2003, 24, 4337-4351.
38. E. Kaemmerer, F. P. Melchels, B. M. Holzapfel, T. Meckel, D. W. Huttmacher and D. Loessner, *Acta Biomater.*, 2014, 10, 2551-2562.
39. C. K. Kuo and P. X. Ma, *Biomaterials*, 2001, 22, 511-521.
40. M. Stiehler, C. Bunger, A. Baatrup, M. Lind, M. Kassem and T. Mygind, *J. Biomed. Mater. Res. A*, 2009, 89, 96-107.
41. Z. D. Shi and J. M. Tarbell, *Ann. Biomed. Eng.*, 2011, 39, 1608-1619.
42. Z. Werb, *Cell*, 1997, 91, 439-442.

43. K. Bott, Z. Upton, K. Schrobback, M. Ehrbar, J. A. Hubbellm, M. P. Lutolf and S. C. Rizzi, *Biomaterials*, 2010, 31, 8454-8464.
44. E. Cukierman, R. Pankov, D. R. Stevens and K. M. Yamada, *Science*, 2001, 294, 1708-1712.
45. P. Agarwal, H. Wang, M. Sun, J. Xu, S. Zhao, Z. Liu and X. He, *ACS Nano*, 2017, 11, 6691-6702.
46. A. Folch and M. Toner, *Annu. Rev. Biomed. Eng.*, 2000, 2, 227-256.
47. L. Filipponi, P. Livingston, O. Kašpar, V. Tokárová, and D. V. Nicolau, *Biomed Microdevices*, 2016, 18, 9.
48. N. Tanaka, H. Ota, K. Fukumori, J. Miyake, M. Yamato, and T. Okano, *Biomaterials*, 2014, 35, 9802-9810.
49. J. Tien, C. M. Nelson, and C. S. Chen, *Proc. Natl. Acad. Sci.*, 2002, 99, 1758-1762.
50. D. Falconnet, G. Csucs, H. M. Grandin, and M. Textor, *Biomaterials*, 2006, 27, 3044-3063.
51. E. Delamarche, A. Bernard, H. Schmid, A. Bietsch, B. Michel, and H. Biebuyck, *J Am. Chem. Soc.*, 1998, 120, 500-508.
52. B. Guillotin, A. Souquet, S. Catros, M. Duocastella, B. Pippenger, S. Bellance, and F. Guillemot, *Biomaterials*, 2010, 31, 7250-7256.
53. R. Gaebel, N. Ma, J. Liu, J. Guan, L. Koch, C. Klopsch, and F. Wang, *Biomaterials*, 2011, 32, 9218-9230.

Laser Printing-Enabled Direct Creation of Cellular Heterogeneity in Lab-on-a-Chip Devices



Laser-induced forward transfer for printing of cellular heterogeneity in organ-on-a-chip devices